Desalination 400 (2016) 18–24

Contents lists available at ScienceDirect

Desalination

journal homepage: www.elsevier.com/locate/desal

Energy consumption analysis of constant voltage and constant current operations in capacitive deionization

Yatian Qu [a,b], Patrick G. Campbell [b], Lei Gu [c], Jennifer M. Knipe [b], Ella Dzenitis [d], Juan G. Santiago [a,*], Michael Stadermann [b,*]

[a] Department of Mechanical Engineering, Stanford University Stanford, CA 94305, USA
[b] Lawrence Livermore National Laboratory, 7000 East Avenue, Livermore, CA, USA
[c] Department of Electrical Engineering, Stanford University Stanford, CA 94305, USA
[d] Dartmouth College, Hanover, NH 03755, USA

HIGHLIGHTS

- Two circuit models useful in elucidating constant current (CC) versus constant voltage (CV) CDI energy consumption dynamics.
- CC mode consumes significantly less energy than CV mode for equal amounts of input charge and identical charging duration.
- CC mode has approximately same salt removal as CV and avoids initial high-power resistive dissipation of CV mode.

GRAPHICAL ABSTRACT

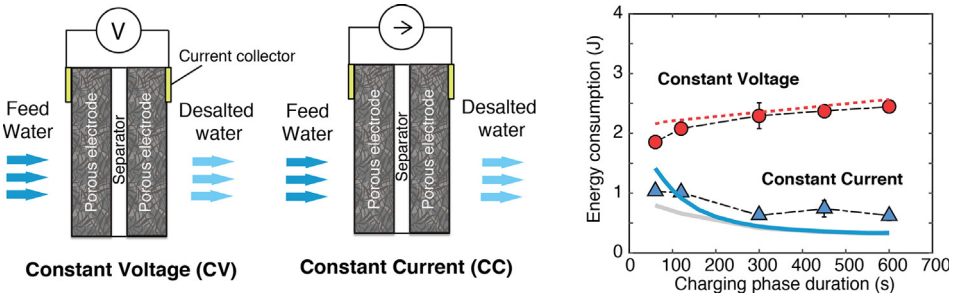

ARTICLE INFO

Article history:
Received 2 June 2016
Received in revised form 9 August 2016
Accepted 15 September 2016
Available online xxxx

Keywords:
Capacitive deionization
Energy consumption
Constant current and constant voltage

ABSTRACT

We report our studies to compare energy consumption of a CDI cell in constant voltage (CV) and constant current (CC) operations, with a focus on understanding the underlying physics of consumption patterns. The comparison is conducted under conditions that the CV and CC operations result in the same amounts of input charge and within identical charging phase durations. We present two electrical circuit models to simulate energy consumption in charging phase: one is a simple RC circuit model, and the other a transmission line circuit model. We built and tested a CDI cell to validate the transmission line model, and performed a series of experiments to compare CV versus CC operation under the condition of equal applied charge and charging duration. The experiments show that CC mode consumes energy at 33.8 kJ per mole of ions removed, which is only 28% of CV mode energy consumption (120.6 kJ/mol), but achieves similar level of salt removals. Together, the models and experiment support our major conclusion that CC is more energy efficient than CV for equal charge and charging duration. The models also suggest that the lower energy consumption of CC in charging is due to its lower resistive dissipation.

1. Introduction

Capacitive deionization (CDI) is an emerging technique for water desalination. It is especially promising for treating water with low and moderate salt concentration, also known as brackish water [1,2]. The

* Corresponding authors.
E-mail addresses: juan.santiago@stanford.edu (J.G. Santiago), stadermann2@llnl.gov (M. Stadermann).

http://dx.doi.org/10.1016/j.desal.2016.09.014
0011-9164/

key component of a CDI cell is a pair of porous carbon electrodes. Salt ions are removed from water and held electrostatically at pore surfaces. CDI operates at low voltage (<1.4 V) and low pressure, and has the potential to be cost effective and energy efficient.

Energy consumption is a crucial factor when comparing CDI to state of the art desalination technology, reverse osmosis (RO) [3,4]. A CDI cell can be operated at various charging modes including constant voltage (CV) [5–8] and constant current (CC) [7,9–15]. Different modes lead to discrepant energy consumption patterns. Zhao et al. [15] and Choi [16] reported lower energy consumption for CC-operation than CV-operation for membrane capacitive deionization (MCDI) cells. Kang et al. demonstrated that CC mode consumed 26% -30% less energy than that consumed in CV mode with the same amount of ions removed [17]. Recently, Han et al. showed that CV mode consumed approximately 50% more energy than CC mode, and only 5.7% of the total energy consumption in charging process in CV mode was recovered in contrast to up to 40% in CC mode [12]. Although these experimental observations have suggested that CC mode is more energy efficient, a thorough understanding of why CC mode consumes less energy than CV mode is missing. Kang et al. attributed lower energy consumption of CC to its overall lower cell voltage [12]. The work we present here will show that the latter argument is ambiguous and strictly inaccurate since the energy saving of CC operation over CV (for equal charge and charging duration) is insensitive to operational voltages of CC. Further, as with most studies, there is no significant effort to make "fair comparison" between the two modes (e.g., charging to same net charge for equal time).

Fundamentally, energy dissipates as currents pass through resistances in the form heat. The underlying reason that CC consumes less energy than CV is that, in CC operation, the cell dissipates less power through resistive components, as CC has better control of charging currents. Another energy consumption advantage of CC is that CC decreases the time the cell operates under conditions where electrode-to-solution potentials result in parasitic (Faraday) reactions. We also note that all of the aforementioned studies report energy consumption as the amount of electrical energy applied to a CDI cell in charging. Instead, we here define this "Energy input" a value equal to the time integral of charging power (product of charging voltage and current) of the external power source to a CDI cell. Note that it is inaccurate to equate energy input and energy consumption. Only a fraction of the energy input is dissipated/consumed by the cell, a second important fraction is instead stored within the cell as capacitive energy in electrical double layers. This stored energy is recoverable (not part of "energy consumed"). Experimentally, will quantify recoverable energy using a low current discharge. Under low current discharge, energy dissipated by resistances and parasitic reactions in the cell are small compared to the recoverable electrical capacitance. Such recovered energy can be stored externally (e.g. in supercapacitors or batteries) or used by other devices, including other CDI cells. We advocate to the community that energy consumption of CDI processes should be the unrecoverable, dissipated energy during an operation cycle, and should not include stored capacitive energy.

In this study, we present two electrical circuit models to simulate and compare energy consumption of CC and CV operation modes. The first model is a simple RC circuit model, and the second is an experimentally validated circuit model based on classic transmission line theory to simulate a capacitance and resistance network. We validate simulation results by performing experiments with a flow-through CDI (ftCDI) cell made of hierarchical carbon aerogel monoliths (HCAMs) electrodes, as shown in Fig. 1a and b. We demonstrate that CC consumes less energy than CV with the same amount of charge transferred and within the identical operation timespan. For our comparison, the two modes also achieve similar charge efficiency. We attribute lower consumption of CC mode to less resistive dissipation in the charging process. As far as we know, our work is the first study centered on the underlying physics of why CC consumes less energy than CV operations for CDI cells. Although we here use ftCDI cell as our model system, our results and conclusions are applicable to flow-between CDI cells and operations. We note that our study might not apply to membrane CDI (MCDI) because other energy loss mechanisms in MCDI, such as energy loss associate with ions overcoming membrane barriers, are not captured by our models and analysis.

2. Energy consumption analysis

2.1. Simple RC circuit analysis

For first-order analysis of energy dissipation in charging, we model a CDI cell as a simple RC circuit: a capacitor C in series with a resistor R, as shown in Fig. 1c. This model is perhaps the simplest but still powerful for understanding energy consumption associated with charging and discharging process in CDI. Here, the capacitor C represents the total electrical double layer capacitance for salt adsorption and the resistor R represents an equivalent total resistance of the cell. To create the simplest model which nevertheless offers valuable insight, we here assume that the capacitance and resistance remain the same during charging or discharging process. We consider comparisons where we charge over the same time and equal amounts of charge.

Fundamentally, energy dissipates through the resistive components of a CDI cell in the form of heat. The dissipation power of a CDI cell is proportional to its resistance and the square of response current: $P = I^2R$. Here the current response I is determined by electrical operation modes, and CC and CV modes have distinguished energy consumption patterns as we further discuss in the paper.

We analyze energy consumption of CV and CC operations under the conditions of finite charging time and the same amount of input charge. For CV operation, the current response of a CDI cell is

$$I(t) = \frac{V_{CV}}{R} e^{-\frac{t}{RC}} \tag{1}$$

Here V_{CV} is the constant voltage applied to the CDI cell. R is the total equivalent resistance and C is the total double layer capacitance.

The instantaneous dissipation power is then

$$P(t) = I(t)^2 R = \frac{V_{CV}^2}{R} e^{-2t/RC} \tag{2}$$

If the cell is charged to finite time t, the charge transferred to a CDI cell and the accumulated dissipated energy are

$$q_{CV}(t) = \int_0^t \frac{V_{CV}}{R} e^{-t/RC} dt = V_{CV} C\left(1 - e^{-\frac{t}{RC}}\right), \tag{3}$$

$$E_{CV}(t) = \int_0^t P(t) dt = \int_0^t \frac{V_{CV}^2}{R} e^{-2t/RC} dt = \frac{1}{2} C V_{CV}^2 \left(1 - e^{-\frac{2t}{RC}}\right). \tag{4}$$

As per Eq. (4), for finite charging time and fixed C and V_{CV}, CV energy consumption is a strong function of resistance R and charging time t. We note that if a CDI cell is charged to infinite time, the energy consumption is $CV^2/2$. However, in practical applications, we cannot and would not want to charge a CDI cell for very long times as this leads to very slow salt removal rate and poor water recovery. We here use a total resistance R as 7.64 Ω and capacitance C as 3.84 F, based on values characterized for our CDI cell. We plot energy consumption of CV mode as a function of time in Fig. S-1a.

For CC operational mode, the dissipated energy of a RC circuit is simply:

$$E_{cc}(t) = I_{CC}^2 Rt. \tag{5}$$

For a fair comparison, we charge a cell at CC mode for a duration of time t such that the charge transferred is the same as that in CV mode within the identical timespan. As we later show that electric charge is

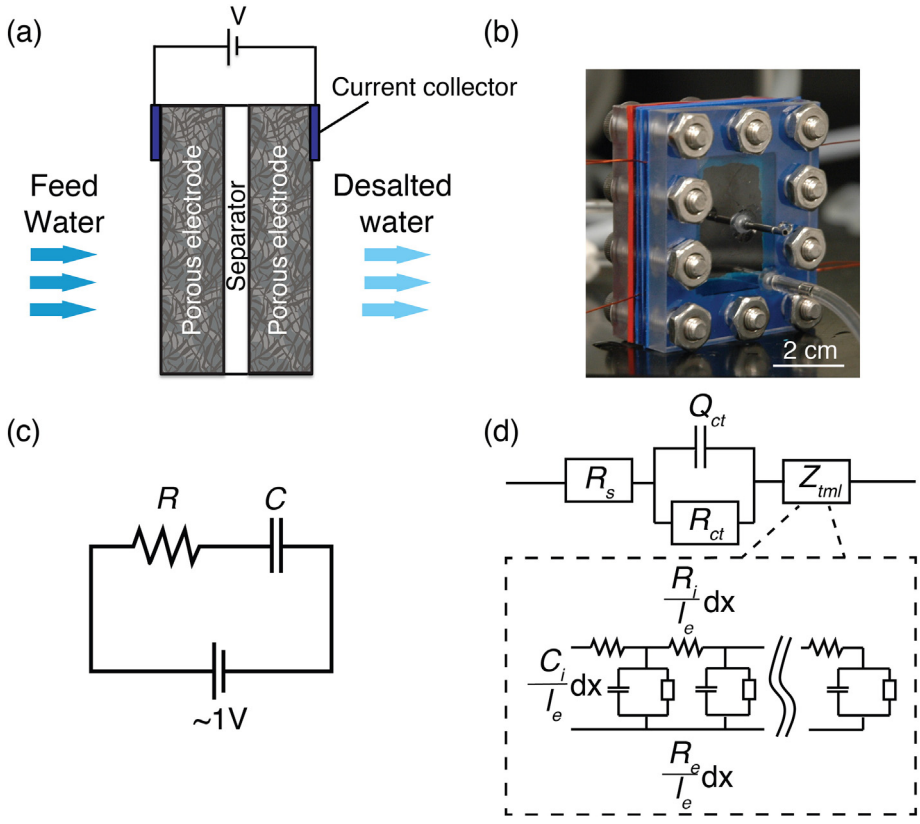

Fig. 1. (a) Schematic and (b) image of a flow-through CDI cell. The cell consists a pair of 300 μm thick porous carbon electrodes, an 80 μm porous dielectric separator, two metal current collectors and wires. (c) Simple RC circuit model for a CDI cell. (d) Equivalent circuit of a CDI cell based on transmission line impedance model.

a good proxy for salt removal, these comparison conditions imply a similar salt removal rate for both CV and CC.

The unique value of equivalent constant charging current I_{CC} is then

$$I_{CC} = \frac{q_{CV}}{t} = \frac{V_{CV}C\left(1-e^{-\frac{t}{RC}}\right)}{t}. \quad (6)$$

Here q_{CV} is the accumulated charge and V_{CV} is the voltage applied in the counterpart CV mode to which we compared.

The energy consumption for the equivalent CC mode described above is:

$$E_{CC}(t) = \int_0^t I_{CC}^2 R dt = I_{CC}^2 R \int_0^t dt = \frac{V_{CV}^2 C^2 R}{t}\left(1-e^{-t/RC}\right)^2. \quad (7)$$

This equivalent energy consumption is again a strong function of resistance R and charging time t. We plot E_{CC} as a function of time in Fig. S-2a.

Combining Eqs. (4) and (7), the ratio of energy consumption of constant voltage and constant current is

$$\frac{E_{CC}}{E_{CV}}(t) = \frac{2RC}{t}\frac{1-e^{-\frac{t}{RC}}}{1+e^{-\frac{t}{RC}}}. \quad (8)$$

Perhaps surprisingly, this ratio is always smaller than unity regardless of the values of resistance R and capacitance C (Fig. S-1b). This simple model therefore suggests CC operation always consumes less energy than CV for the same amounts of input charge and for identical timespans. In addition, energy consumption for either CV or CC mode strongly depends on the equivalent total resistance R.

2.2. Transmission-line based circuit model and simulations in LTspice

The resistive and capacitive components in a CDI cell are much more complex than a simple RC circuit. The simple RC circuit is unable to capture the non-uniform charging dynamics of a porous electrode, and it does not include charge loss mechanisms, such as parasitic reactions on electrode surface [4,8,18–20]. To further understand the energy consumption in charging process in a CDI cell, we use an equivalent circuit model based on classical transmission line (TL) theory. Transmission line impedance models are commonly used to simulate resistance and capacitance network in porous electrodes [3,21–24]. In our model, we have a setup resistance (ionic resistance of the solution in the separators and electrical resistance of current collectors and wires), a contact resistance to model the contact between current collectors and porous electrodes, and two porous electrodes each modeled as a TL with 20 resistor-capacitor units (Fig. S-2). Each resistor-capacitor unit consists of an EDL capacitor element, an ionic resistance element, an electrode resistance element, and a leakage resistance element which models parasitic reactions. We use a voltage-dependent non-linear relationship that follows Butler-Volmer equation for leakage resistors. We assume constant EDL capacitance and ionic resistance in our simulations because there is no significant ion depletion during charging at the feed concentrations we use in experiments. Further, constant capacitance and ionic resistance elements generate simulation results which sufficiently well match experimental data (see Results and discussion). We published a simpler version of this model in our previous study [3]. We here perform simulations with our equivalent circuit model in an integrated circuit simulator LTspice to study dynamic current and voltage responses and evaluate energy dissipations. Simulation conditions are determined by experiments. All the resistive and capacitive values in the LTspice model match those in experiments, as we later describe in

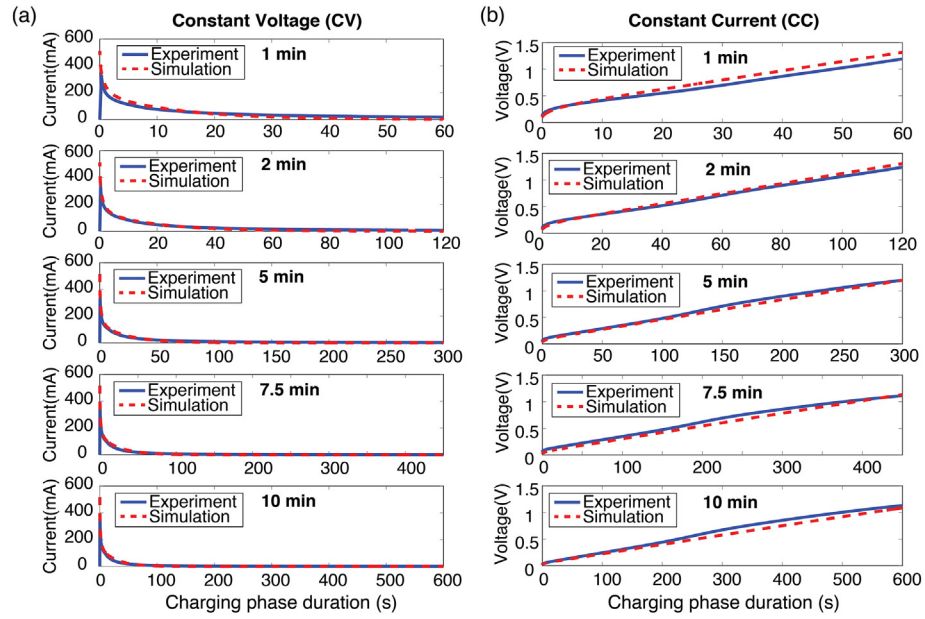

Fig. 2. (a) Experimental and simulated current responses of a CDI cell under 1 V CV operation with charging phase durations of 1, 2, 5, 7.5 and 10 min. (b) Experimental and simulated voltage responses of a CDI cell under equivalent CC operations with charging phase durations of 1, 2, 5, 7.5 and 10 min. Solid blue lines represent experimental data and red dash lines represent simulation results. (For interpretation of the references to color in this figure legend, the reader is referred to the web version of this article.)

Material and methods. Fig. 2 compares simulated cell responses to experimental data in CV and CC modes, which shows that transmission line based LTspice model captures charging dynamics of a CDI cell well.

We determine the energy consumption of CC and CV modes in modeling by summing up the dissipation energy of all resistive elements, as shown below:

$$E = \sum_{m=1}^{N_i} \int_{t_0}^{t_1} I_{R_{i(m)}}^2 R_{i(m)} dt + \sum_{k=1}^{N_e} \int_{t_0}^{t_1} I_{R_{e(k)}}^2 R_{e(k)} dt + \sum_{n=1}^{N_{leak}} \int_{t_0}^{t_1} I_{R_{leak(n)}}^2 R_{leak(n)} dt + \int_{t_0}^{t_1} I_{R_s}^2 R_s dt + \int_{t_0}^{t_1} I_{R_{ct}}^2 R_{ct} dt, \quad (9)$$

where t_0 and t_1 represent start and end time points of charging process. $R_{i(m)}$ and $R_{e(k)}$ are transmission line resistor elements representing ionic resistance inside pores and electrical bulk resistance of porous materials. N_i and N_e are the numbers of R_i and R_e elements in LTspice simulation, respectively. In our model, we have $N_i = 38$ and $N_e = 40$ (arbitrarily chosen). $R_{leak(n)}$ simulates parasitic reactions across EDL capacitor. N_{leak} is the number of $R_{leak(n)}$ element in the model and we have $N_{leak} = 40$. R_{ct} is the contact resistance between current collector and porous electrode. R_s is the setup resistance as we defined earlier.

3. Material and methods

3.1. Flow-through CDI cell

We fabricated a flow-through CDI cell design using two blocks of hierarchical carbon aerogel monoliths (HCAMs) material [25–28] with area of 2 × 3 cm and thickness of 300 μm, for CV and CC comparison experiments, as shown in Fig. 1a and b. We used an 80 μm thick hydrophilic PTFE membrane filter (JCWP04700, EMD Millipore, Billerica, MA) as a separator to insulate between the two electrodes. We used silver epoxy to create intimate electrical contacts between HCAM electrodes and copper wires [3]. The two porous electrodes and a separator were stacked into an assembly and glued on to a polycarbonate frame using epoxy. This assembly was then sandwiched between two 4.2 × 5.0 × 0.6 cm polycarbonate endplates with 630 μm silicone rubber sheets as gaskets. Both endplates were milled to accommodate a tubulation as a port to flow water. The cell was assembled using ten bolts. The cell assembly frame and housing parts were fabricated from polycarbonate.

3.2. ftCDI cell characterization

We characterized capacitance of our ftCDI cell by performing cyclic voltammetry using BioLogic SP-300 potentiostat (Bio Logic Science Claix, France). Apparent capacitances obtained from cyclic voltammetry are well known to depend on scan rates, and slow scan rates generate capacitance readings closer to equilibrium capacitances [29–31]. To accurately evaluate the equilibrium capacitance in a CDI cell, we performed cyclic voltammetry at a slow scan rate of 1.67 mV/s, as shown in Fig. 3-S. We then extracted capacitance from cyclic voltammetry data and applied it as an input parameter to LTspice model.

The resistances of the entire CDI cell were characterized by electrochemical impedance spectroscopy (EIS) using a potentiostat [3]. EIS was performed in a two-terminal configuration without a reference electrode since the electrodes of the cell were symmetric. We applied a 10 mV amplitude sinusoidal potential perturbation and scanned over a frequency range from 700 kHz to 10 mHz at 0 V bias. During electrochemical tests, the cell was filled with 100 mM NaCl. We waited 30 min before performing EIS measurements to allow the cell to equilibrate with the sodium chloride solution. We extracted setup resistance R_s, contact resistance R_{ct} and ionic resistance inside porous electrodes R_i from Nyquist plot of EIS responses (Fig. S-4) and then used them as parameters in LTspice simulations.

We characterized parasitic reaction currents by performing constant voltage experiments at 0.2, 0.4, 0.6, 0.8, 1.0 and 1.2 V while flowing feed solution through the cell, and recorded leakage currents after 10 min of charging. 10 min is much longer than the CDI cell's RC time constant (about 25 s). Therefore, we assume that the currents we observed at 10 min were due to parasitic reactions, not because of EDL charging. We then fitted leakage currents data to obtain a Bulter-Volmer equation to characterize voltage-dependent parasitic reactions (Fig. S-5).

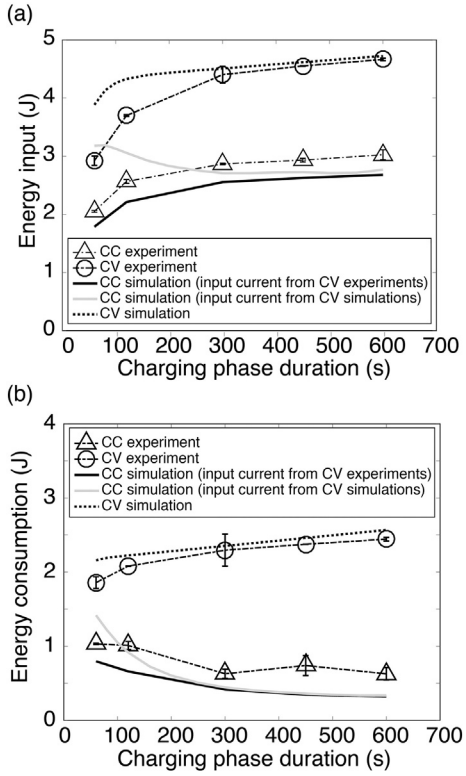

Fig. 3. Comparison of (a) energy input and (b) energy consumption of a CDI cell in CV or CC mode versus charging phase durations of 1, 2, 5, 7.5 and 10 min. CV and CC modes were operated under the conditions of the same input electric charge and identical charging times. The dotdash line with circle markers represents experimental data for CV operation. The dotdash line with triangular markers represents CC experimental data. The shortdash line is simulation results for CV mode. Black and light gray solid lines are simulation data for CC mode using input current from CV experiments and simulation data for CC mode using input current from corresponding CV simulations.

3.3. Constant voltage and constant current charging experiments

We performed CV and CC experiments using our CDI cell with 100 mM NaCl. With this concentration, there is no significant ion depletion in the cell during charging. We used a Biologic SP-300 potentiostat (Bio Logic Science Claix, France) to supply voltage or current and monitor electrical responses. A flow-through conductivity sensor (Edaq, Denistone East, Australia) was attached to the CDI cell downstream to measure the conductivity of effluent solution. We used a syringe pump (Harvard Apparatus syringe pump, Holliston, MA) to flow feed solution through the cell at 0.24 mL/min. We waited 30 min before starting experiments to allow the cell to equilibrate with sodium chloride solutions.

We first performed CV experiments at 1 V with charging phase durations of 1, 2, 5, 7.5 and 10 min. We obtained the total amounts of charge transferred from potentiostat to the CDI cell by integrating current responses over charging times. To satisfy the conditions of the same input charge and identical timespan, we determined the charging currents for counterpart CC experiments by dividing accumulated charge measured in the CV experiment by total charging time. We then performed counterpart CC experiments for 1, 2, 5, 7.5 and 10 min with the corresponding equivalent currents. For each experiment, we performed two charging and discharging cycles. In both cycles, the charging steps followed preset experiment conditions. For discharging in the first cycle, we drew a very small discharging current (2 mA) from the cell to extract an estimate of stored energy in EDL. In second cycle, we held the cell at open circuit state for 15 min after charging to flush desalted water in order to obtain more accurate estimates of salt removal. We then grounded the cell for 10 min to ensure complete regeneration of electrodes prior to the next charging.

4. Results and discussion

4.1. Model validation

As discussed above, the parameters of our LTSpice model are determined using independent experiments using cyclic voltammetry, EIS and leakage current experiments. We then use our LTSpice model to make predictions of the CDI cell in operational modes.

To validate the performance of our LTSpice model, we compared simulated voltage and current responses of the ftCDI cell to experimental data. Fig. 2a shows experimental and simulation data of current responses of the cell under 1 V CV operation with 1, 2, 5, 7.5 and 10 min charging phase durations. Fig. 2b shows experimental and simulation data of voltage responses of the CDI cell under corresponding CC conditions with the same set of charging phase durations. Simulation results from LTspice model demonstrate fair agreement with experimental data, especially for longer charging times. This agreement validates the use of a transmission line based circuit model to predict electrical charging dynamics and energy consumptions of a CDI cell. Our primary use of this model will be to study the differences between CC and CV energy dissipation.

For our LTspice circuit model, we chose to implement constant capacitor elements. We view this circuit model as the simplest transmission line model which nevertheless sufficiently captures the physics of CDI operation and helps us compare CC versus CV operations. In the Supplementary Information document, we show cyclic voltammetry characterizations (Fig. S-3) which explore the net capacitances of our cell. The cyclic voltammetry data capture some voltage dependence of differential capacitance. However, we avoided fitting such data to obtain capacitance versus voltage relations since it is difficult to decouple the effects of capacitance changes versus parasitic reactions in the system. We do not know of a straight forward manner to decouple these confounding effects. Future work could include exploring the relative importance of changes in capacitance versus parasitic reaction effects, and including extending our model to include voltage-dependent capacitances. Our experience so far in exploring this issue is that constant capacitance models are likely sufficiently accurate for operation at higher ionic strengths of the inlet (order 100 mM salt concentration or greater).

4.2. Energy input and energy consumption comparison

We obtain energy inputs to CDI cell by integrating the product of cell voltage and current over charging times, as described by Eq. (10):

$$E_{in} = \int_0^t I_{cell} V_{cell} dt, \tag{10}$$

This energy input calculation applies to either CV or CC operation. In CV mode, V_{cell} is fixed and I_{cell} is the cell's current in response. In CC mode, V_{cell} is the measured and I_{cell} is fixed. Fig. 3a shows the comparisons of energy inputs of CV and CC modes in experiments and simulations as a function of duration of the charging phase. For each set of data, we first performed CV runs and used measured time-integrated current to calculate electric charge transferred to the cell. We then choose corresponding current values for the CC experiments to source the (unique) applied current to transfer the same charge in the same time as the CV experiment.

Fig. 3a presents two sets of simulations results for CC mode. The first set are predictions of the CC circuit model given the applied (experimental) current. These CC current values therefore ensure the corresponding CC and CV *experiments* have identical electric charge transferred in identical charging phase times. As a reference and comparison, we also show CC circuit model predictions for corresponding

current values which are predicted by the transferred charge predicted by the CV model. The latter data therefore ensure that the CV and CC *predictions* have identical electric charge transferred in identical charging timespans. Note the discrepancy between the latter prediction and experiments for short charging phase durations. We attribute this to the effect of increased ionic resistance in the cell for CV operation. The residence time of flow in the cell (solution volume inside the cell divided by flow rate) is about 56 s. For charging phase duration of this order (or shorter), the rapid initial ionic charge trapping of the CV mode results in a short-term rise in ionic resistance; and such changes are not accounted for in the model (which assumes constant resistances). For longer cycle times, the solution inside the cell is well replenished by the flow and the measured time-average resistance loss are closer to those predicted.

We determine energy consumption for both simulations and experiments. In simulations, energy consumption is calculated as the sum of the dissipation energy of all resistive elements in model (i.e., Equation 9) and dissipation of the parasitic reaction circuit elements. In the experiments, we follow cell charging by discharging at a low current to evaluate energy consumptions (as we described in Material and methods). This low-current discharge lets us estimate recoverable output energy. For the experiments, we therefore estimate energy consumption during charging by subtracting from input energy the following three energy values: recoverable output energy, resistive dissipation energy in discharging, and parasitic reaction energy in discharging. The latter is estimated using our Bulter-Volmer model for parasitic current (see Section S-5). We can express the estimate for energy consumed during charging in the experiments as follows:

$$E = E_{in} - E_{out} - \int_{t1}^{t2} I_{dis}^2 R_{cell} dt - E_{parasitic,dis}. \quad (11)$$

Here, t_1 and t_2 represent start and end time points of discharging phase. E is energy consumption in charging process. E_{in} represents input energy as measured by the potentiostat to the CDI cell. E_{out} is the recoverable output energy from EDL and it is obtained by discharging the cell at a very small constant current. $\int_{t1}^{t2} I_{dis}^2 R_{cell} dt$ represents resistive dissipation associated with small current discharging, where R_{cell} is the total equivalent resistance of the CDI cell and I_{dis} is the discharging current (2 mA in our case). $E_{parastic,dis}$ is the estimate energy consumed by parasitic reactions during discharging. $E_{parastic,dis}$ is the time integral of the product of parasitic current and cell voltage. Note (potentiostat) voltage is expected to be a good estimate of potential across surface charge layers (and therefore the potential parameter in the Bulter-Volmer equation) for such low currents.

Fig. 3b shows simulated and experimental energy consumption of CV and CC operations during charging process. With either fast or slow charging rates, CV consumes significantly higher energy than CC under the condition that the same amounts of charge are transferred to the cell within the identical charging timespans. We note here that the salt removals are comparable in CV and CC experiments, as we discuss further in next section. Our model successfully predicts the same major conclusion that CC is more energy efficient than CV for equal charge and charging phase duration. The model results therefore support the hypothesis that the lower energy consumption of CC in charging is due to its lower resistive dissipation. We note that there is some discrepancy between model and experiments for both the CC and CV cases, particularly for charge phase durations of order 100 s or less. As mentioned above, we attribute this discrepancy to the rapid initial rise of ionic resistance associated with CV operation. Our model does not capture such rapid-changing ionic resistance changes.

4.3. Salt removal comparison

We compare salt removals of CC and CV experiments to investigate if there is a trade-off between energy consumption and salt adsorption capabilities. We calculate salt removed from real-time conductivity measurement of effluent stream. Fig. 4 shows experimentally measured energy consumption normalized by moles of salt removed as a function of charging phase duration. These data clearly demonstrate that CC consumes less energy per moles of salt removed than CV operation. At a charging duration of 10 min, CC mode consumes energy at 33.8 kJ per mole of ions removed, which is only 28% of CV mode energy consumption (120.6 kJ/mol). The inset figure compares the absolute salt adsorptions of CV and CC. Interestingly, CV and CC remove similar amounts of salts for all five charging phase durations (and so electric charge is here a good proxy for salt removal). These observations reinforce the conclusion that CC mode consumes significantly less energy than CV mode, while also achieving a similar level of salt adsorption.

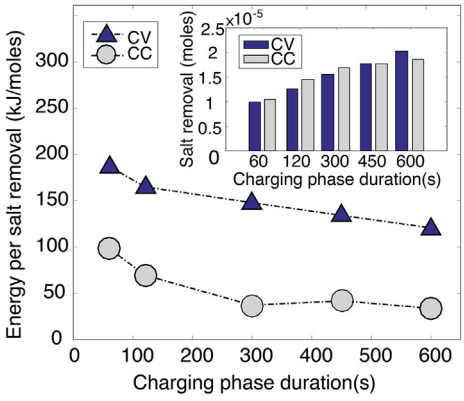

Fig. 4. Energy consumption per mole of salt removal of CV and CC operations from experiments with charging phase durations of 1, 2, 5, 7.5 and 10 min. In the main figure, the dotdash line with blue triangular markers is energy per salt removal of CV operation, whereas the dotdash line with gray circle marker represents CC mode data. Inset figure compares the absolute amounts of salt adsorbed in CV and CC experiments, which indicates similar desalination performance of these two modes. (For interpretation of the references to color in this figure legend, the reader is referred to the web version of this article.)

4.4. Conclusions

We here report our studies on energy consumption of a CDI cell and compare the two most commonly used operation modes: constant voltage (CV) and constant current (CC). The comparison of energy consumption is conducted under the strictly enforced conditions that the CV and CC operations result in the same amounts of input (electric) charge and within identical charging timespans. We have developed a transmission-line based LTspice circuit model to capture electrical dynamics of CDI charging and investigate energy consumption mechanisms. We found that CC mode consumes much less energy than CV mode but achieves similar level of salt removals, and this is due to less resistive dissipation with CC. We focused on energy consumption during the charging process in order to accurately access salt removal and avoid salt contamination of the effluent stream caused by ion desorption at the beginning of a standard discharging step. Isolating charging and discharging steps enables precise evaluation of energy cost per unit of ions removed. We hypothesize that our major conclusion regarding energy consumption (that CC is more energy efficient than CV) applies to the discharging phase and to the entire charge/discharge cycle.

Lastly, we note that the CC operation possesses other advantages over CV apart from lower energy consumption, such as producing constant and adjustable effluent concentrations [9,10,32,33], and limiting charging time spent at substantial oxidizing potentials [8]. Therefore, we advocate the use of CC mode over CV for CDI cell operations to achieve lower energy consumption as well as produce controllable desalted effluent.

Acknowledgments

Yatian Qu would like to thank the Lawrence Scholar program. This work was supported by LLNL LDRD project 15-ERD-068. Work at LLNL was performed under the auspices of the US DOE by LLNL under Contract DE-AC52-07NA27344. Yatian Qu and Juan G. Santiago also gratefully acknowledge support from the TomKat Center for Sustainable Energy at Stanford University.

Appendix A. Supplementary data

Supplementary data to this article can be found online at http://dx.doi.org/10.1016/j.desal.2016.09.014.

References

[1] M.E. Suss, S. Porada, X. Sun, P.M. Biesheuvel, J. Yoon, V. Presser, Water desalination via capacitive deionization: what is it and what can we expect from it? Energy Environ. Sci. 8 (2015) 2296–2319.
[2] S. Porada, R. Zhao, A. van der Wal, V. Presser, P.M. Biesheuvel, Review on the science and technology of water desalination by capacitive deionization, Prog. Mater. Sci. 58 (2013) 1388–1442.
[3] Y. Qu, T.F. Baumann, J.G. Santiago, M. Stadermann, Characterization of resistances of a capacitive deionization system, Environ. Sci. Technol. 49 (2015) 9699–9706.
[4] A. Hemmatifar, J.W. Palko, M. Stadermann, J.G. Santiago, Energy breakdown in capacitive desalination, Water Res. (2016).
[5] A. Hemmatifar, M. Stadermann, J.G. Santiago, Two-Dimensional porous electrode model for capacitive deionization, 2015.
[6] Y. Bian, P. Liang, X. Yang, Y. Jiang, C. Zhang, X. Huang, Using activated carbon fiber separators to enhance the desalination rate of membrane capacitive deionization, Desalination 381 (2016) 95–99.
[7] T. Kim, J.E. Dykstra, S. Porada, A. van der Wal, J. Yoon, P.M. Biesheuvel, Enhanced charge efficiency and reduced energy use in capacitive deionization by increasing the discharge voltage, J. Colloid Interface Sci. 446 (2015) 317–326.
[8] X. Gao, A. Omosebi, J. Landon, K. Liu, Surface charge enhanced carbon electrodes for stable and efficient capacitive deionization using inverted adsorption–desorption behavior, Energy Environ. Sci. 8 (2015) 897–909.
[9] R. Zhao, O. Satpradit, H.H. Rijnaarts, P.M. Biesheuvel, A. van der Wal, Optimization of salt adsorption rate in membrane capacitive deionization, Water Res. 47 (2013) 1941–1952.
[10] T. Kim, J. Yoon, CDI ragone plot as a functional tool to evaluate desalination performance in capacitive deionization, RSC Adv. 5 (2015) 1456–1461.
[11] R. Zhao, S. Porada, P.M. Biesheuvel, A. van der Wal, Energy consumption in membrane capacitive deionization for different water recoveries and flow rates, and comparison with reverse osmosis, Desalination 330 (2013) 35–41.
[12] L. Han, K.G. Karthikeyan, K.B. Gregory, Energy consumption and recovery in capacitive deionization using nanoporous activated carbon electrodes, J. Electrochem. Soc. 162 (2015) E282–E288.
[13] E. Garcia-Quismondo, R. Gomez, F. Vaquero, A.L. Cudero, J. Palma, M. Anderson, New testing procedures of a capacitive deionization reactor, Phys. Chem. Chem. Phys. 15 (2013) 7648–7656.
[14] Y.A.C. Jande, W.S. Kim, Desalination using capacitive deionization at constant current, Desalination 329 (2013) 29–34.
[15] R. Zhao, P.M. Biesheuvel, A. van der Wal, Energy consumption and constant current operation in membrane capacitive deionization, Energy Environ. Sci. 5 (2012) 9520.
[16] J.-H. Choi, Comparison of constant voltage (CV) and constant current (CC) operation in the membrane capacitive deionisation process, Desalin. Water Treat. 56 (2014) 921–928.
[17] J. Kang, T. Kim, K. Jo, J. Yoon, Comparison of salt adsorption capacity and energy consumption between constant current and constant voltage operation in capacitive deionization, Desalination 352 (2014) 52–57.
[18] A.M. Oickle, H.A. Andreas, Examination of water electrolysis and oxygen reduction as self-discharge mechanisms for carbon-based, Aqueous Electrolyte Electrochemical Capacitors, The Journal of Physical Chemistry C 115 (2011) 4283–4288.
[19] Y. Diab, P. Venet, H. Gualous, G. Rojat, Self-discharge characterization and modeling of electrochemical capacitor used for power electronics applications, IEEE Transactions on Power Electronics 24 (2009) 510–517.
[20] M. Kaus, J. Kowal, D.U. Sauer, Modelling the effects of charge redistribution during self-discharge of supercapacitors, Electrochim. Acta 55 (2010) 7516–7523.
[21] M.E. Suss, T.F. Baumann, M.A. Worsley, K.A. Rose, T.F. Jaramillo, M. Stadermann, J.G. Santiago, Impedance-based study of capacitive porous carbon electrodes with hierarchical and bimodal porosity, J. Power Sources 241 (2013) 266–273.
[22] R.D. Levie, On porous electrodes in electrolyte solutions IV, Electrochim. Acta 9 (1964) 1231–1245.
[23] G.J. Brug, A.L.G. van den Eeden, M. Sluyters-rehbach, J.H. Sluyters, The analysis of electrode impedance complicated by the presence of a constant phase element, J. Electroanal. Chem. 176 (1984) 275–295.
[24] D.B. Robinson, Optimization of power and energy densities in supercapacitors, J. Power Sources 195 (2010) 3748–3756.
[25] T.F. Baumann, M.A. Worsley, T.Y.-J. Han, J.H. Satcher, High surface area carbon aerogel monoliths with hierarchical porosity, J. Non-Cryst. Solids 354 (2008) 3513–3515.
[26] J. Biener, M. Stadermann, M. Suss, M.A. Worsley, M.M. Biener, K.A. Rose, T.F. Baumann, Advanced carbon aerogels for energy applications, Energy Environ. Sci. 4 (2011) 656.
[27] M.E. Suss, T.F. Baumann, W.L. Bourcier, C.M. Spadaccini, K.A. Rose, J.G. Santiago, M. Stadermann, Capacitive desalination with flow-through electrodes, Energy Environ. Sci. 5 (2012) 9511.
[28] M.E. Suss, P.M. Biesheuvel, T.F. Baumann, M. Stadermann, J.G. Santiago, In situ spatially and temporally resolved measurements of salt concentration between charging porous electrodes for desalination by capacitive deionization, Environ. Sci. Technol. 48 (2014) 2008–2015.
[29] H. Wang, A. Thiele, L. Pilon, Simulations of cyclic voltammetry for electric double layers in asymmetric electrolytes: a generalized modified Poisson–Nernst–Planck model, J. Phys. Chem. C 117 (2013) 18286–18297.
[30] H. Wang, L. Pilon, Physical interpretation of cyclic voltammetry for measuring electric double layer capacitances, Electrochim. Acta 64 (2012) 130–139.
[31] M.D. Stoller, R.S. Ruoff, Best practice methods for determining an electrode material's performance for ultracapacitors, Energy Environ. Sci. 3 (2010) 1294.
[32] M.W. Saleem, Y.A.C. Jande, M. Asif, W.-S. Kim, Hybrid CV-CC operation of capacitive deionization in comparison with constant current and constant voltage, Sep. Sci. Technol. 51 (2016) 1063–1069.
[33] S. Kim, J. Lee, C. Kim, J. Yoon, Na2FeP2O7 as a novel material for hybrid capacitive deionization, Electrochim. Acta 203 (2016) 265–271.

Energy consumption analysis of constant voltage and constant current operations in capacitive deionization

Supporting information

Yatian Qu,[a,b] *Patrick G. Campbell,*[b] *Lei Gu,*[c] *Jennifer M. Knipe,*[b] *Ella Dzenitis,*[d] *Juan G. Santiago*[a]* *and Michael Stadermann*[b]*

[a] Department of Mechanical Engineering, Stanford University Stanford, CA 94305, USA

[b] Lawrence Livermore National Laboratory, 7000 East Avenue, Livermore, CA, USA.

[c] Department of Electrical Engineering, Stanford University Stanford, CA 94305, USA

[d] Dartmouth College, Hanover, NH, 03755, USA

*To whom correspondence should be addressed. E-mails: juan.santiago@stanford.edu and stadermann2@llnl.gov

This document contains supplementary information and figures further describing our simple RC circuit model and transmission line (TL) based LTspice model; additional simulation results of constant voltage (CV) and constant current (CC) operations; and

characterization of capacitance, resistances and parasitic reactions of flow-through capacitive deionization (ftCDI) cell.

- S-1: Simulation results from a simple RC circuit
- S-2: LTSpice model description
- S-3: Cyclic voltammetry to evaluate charging capacitances
- S-4: Electrochemical impedance spectroscopy to measure resistances
- S-5: Characterization and modeling of parasitic reactions
- S-6: Comparison of input charge from experiments and simulations
- S-7: CDI cell electrode salt adsorption capacities

S-1 Simulation results from a simple RC circuit

We here further describe our simple RC circuit model of a CDI cell to compare energy consumption of CV and CC modes, as a first-order of analysis. Our experiments suggest our cell has a total resistance R of 7.64 Ω and electrical double layer capacitance C of 3.84 F. Energy consumption of CV and CC modes using the simple RC circuit are evaluated by Equation 4 and 7 in the main text, under the conditions of the same amounts of input charge and identical timespans. Figure S-1a presents simulated energy consumption with charging phase durations from 60 to 600 s, and it shows that CV consumes significantly more energy than CC, especially with longer charging times. Figure S-1b shows the simulated consumption ratios of CC to CV.

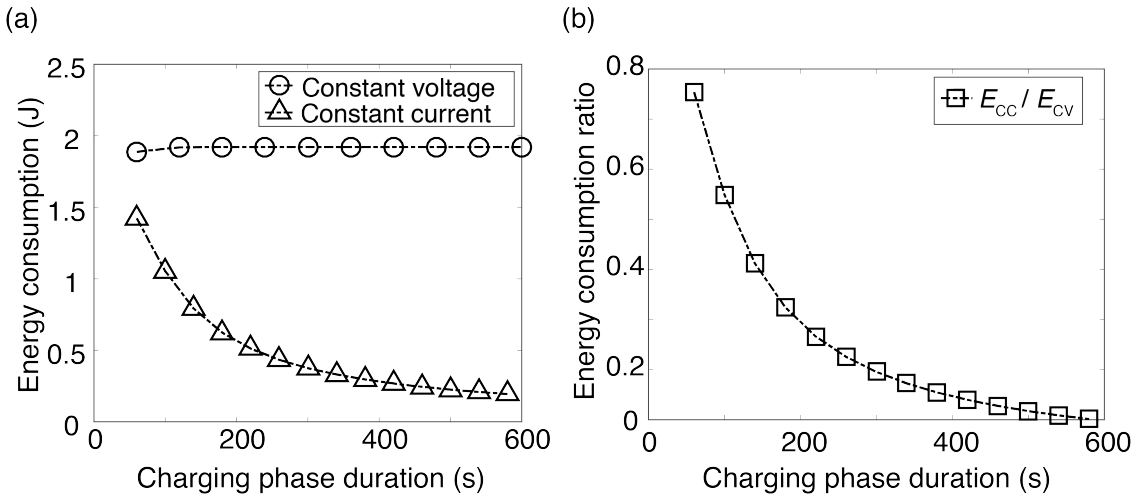

Figure S-1. a) Simulated energy consumption of a CDI cell using simple RC circuit in charging process with CV and CC modes. b) Simulated energy consumption ratio of CC to CV.

S-2 LTspice model description

We performed LTspice simulations to investigate the charging dynamics and energy consumption of a CDI cell. In our model, we have a setup resistance, a contact resistance, and two electrodes each modeled via a TL with 20 resistor-capacitor units (Figure S-2). Each resistor-capacitor unit has a value chosen to reflect the actual resistances or capacitances in our ftCDI cell. We characterized R_s, R_{ct}, and R_i from electrochemical impedance spectroscopy (EIS) data as later described in Section S-4. The characterized R_i and R_e of each electrode are related to the resistance of each element $R_{i1}, R_{i2}, \ldots R_{i19}$ and $R_{e1}, R_{e2}, \ldots R_{e20}$ as follows:

$$R_{i(j)} = R_i/N_i, \quad R_{e(k)} = R_e/N_e \quad (j=1,2, \ldots, 19; k=1,2, \ldots, 20) \tag{S1}$$

where N_i and N_e are the (arbitrarily chosen) number of elements of our discretization. We here chose N_i as 19 and N_e as 20 for each electrode.

The capacitances of each electrode C were measured by cyclic voltammetry of the whole CDI cell, as later described in Section S-3. We assume that capacitance remains constant during charging process. The capacitance of each electrode C is related to each capacitor in the circuit $C_1, C_2, \ldots C_{20}$ as follows:

$$C_{(m)} = C/N_c, \ (m=1,2, \ldots, 20) \tag{S2}$$

we here chose N_c as 20.

We model parasitic reactions of porous electrodes as non-linear resistances R_1, $R_2, \ldots R_{20}$ which follow a Bulter-Volmer equation. In LTspice, a parasitic reaction resistor is in parallel with an EDL capacitor and we used a sub-circuit to model its non-linear behavior. We describe the characterization and modeling of parasitic reactions in Section S-5.

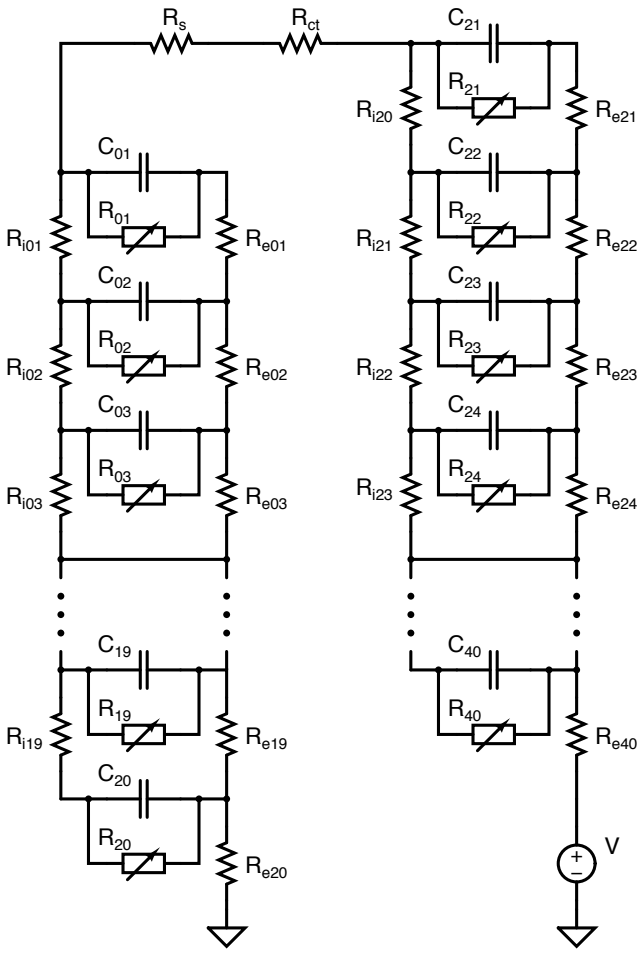

Figure S-2. Schematic of LTspice circuit model used in simulations. We discretized the electrodes using a transmission line modeling approach, and each electrode is represented by 20 resistor-capacitor units. The values of each resistor, capacitor and non-linear parasitic reaction element were determined by independent CDI cell characterization experiments to correctly reflect the properties of our CDI cell.

S-3 Cyclic voltammetry to evaluate charging capacitances

As mentioned in the main text, apparent capacitances of porous electrodes depend on charging rates.[1-3] In order to accurately assess equilibrium EDL capacitance, we performed cyclic voltammetry experiments at a slow scan rate of 1.67 mV/s. Figure S-3 shows measured differential capacitances of our ftCDI cell within a voltage window from -0.2 to 1.3 V. We averaged capacitance values from 0 to 1 V in positive sweeping phases as the capacitance inputs for LTspice models.

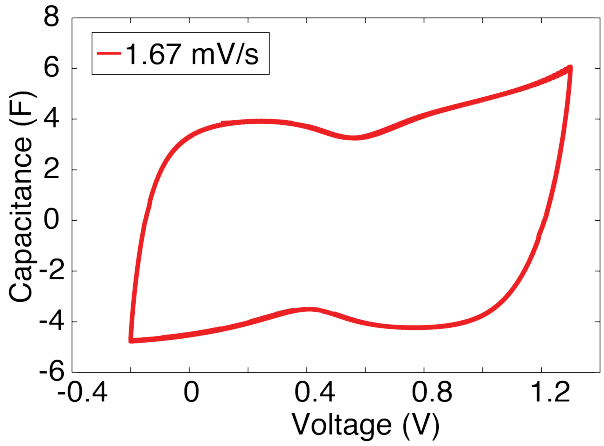

Figure S-3. Cyclic voltammetry of ftCDI cell at scan rate of 1.67 mV/s. The measurement voltage window is from -0.2 to 1.3 V.

S-4 Electrochemical impedance spectroscopy to measure resistances

We characterized resistances of our (entire assembled) ftCDI cell using electrochemical impedance spectroscopy (EIS) using a potentiostat. EIS was performed in a two-terminal configuration without a reference electrode since the electrodes of the cell were symmetric. We applied a 10 mV amplitude sinusoidal potential perturbation and scanned over a frequency range from 700 kHz to 10 mHz at 0 V bias. During electrochemical tests, the cell was filled with 100 mM NaCl. Figure S-4 shows Nyquist plot of EIS response of our ftCDI cell. We extract the values of R_s, R_{ct}, and R_i from the plot as shown in Figure S-4. [4, 5]

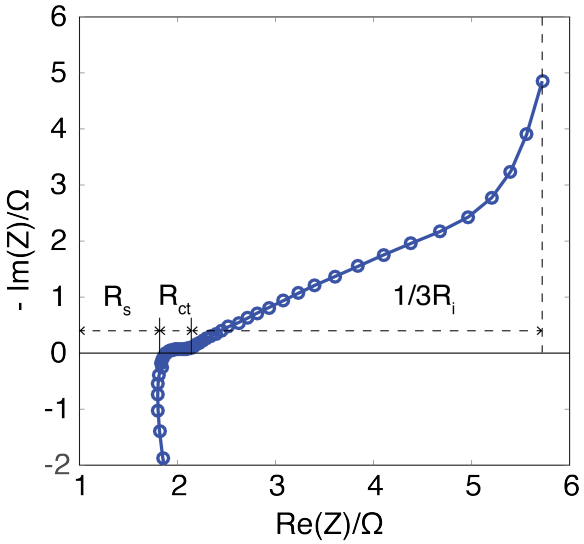

Figure S-4. Nyquist plot of ftCDI cell measured using electrochemical impedance spectroscopy for frequencies within 700 kHz to 10 mHz. The values of R_s, R_{ct}, and R_i are distances along the real axis and are denoted as the labeled line segments flanked by asterisks.

S-5 Characterization and modeling of parasitic reactions

We characterized parasitic reaction currents by performing constant voltage experiments at 0.2, 0.4, 0.6, 0.8, 1.0 and 1.2 V while flowing feed solution through the cell, and recorded leakage currents after 10 min of charging. We then fitted these leakage current data to characterize the parasitic reactions.

In our LTspice model, there are 20 leakage resistor elements in parallel with EDL capacitors for each electrode. Therefore, we divide the measured leakage currents by 20 to obtain current flowing through each resistor. These leakage currents are measured after 10 min of charging, so we can expect the voltage drops across each capacitor element (and therefore each leakage resistor element) to be approximately uniform. We therefore characterize the leakage current voltage using a single value applicable to the cell under these conditions. The voltage across a leakage resistor is obtained by subtracting an ohmic drop of setup resistance and contact resistance from cell voltage and then dividing this by two, as shown in Equation S3.

$$V_{leak} = ½ (V_{cell} - I_{cell} (R_s + R_{ct})) \quad \text{(S3)}$$

We fit parasitic currents data to characterize its voltage dependence. First, we assume that there is a turn-on voltage for parasitic reactions and we define it as V_o. We also assume that, below threshold voltage V_o, the leakage resistor behaves as a large constant resistor with a value of 50 kΩ. When the voltage is above threshold, the leakage resistor behaves non-linearly and follows Bulter-Volmer equation. Equation S4 shows the fit:

$$I_{leak} = \frac{V_0}{50k} e^{\left(\alpha(-V_0+V)\right)} \quad \text{(S4)}$$

We obtained fitting parameters V_o as 0.145 V and α as 7.12 (1/V). In implementing this relation into the model for CDI cell operation, the variable V is then the local, element-specific voltage for each leakage resistor element. We note here that we adopt a modified version of Bulter-Volmer equation because as we found it to be compatible with subcircuit implementation and solutions performed using LTspice.

Our parasitic reaction model has a Tafel slope as 320 mV/decade. In literature, oxygen reduction is usually reported to have two Tafel slopes, 60 mV/decade or 120 mV/decade, depending on the electrode materials and on the potential range.[6]. Our Tafel slope indicates slower kinetics than reported numbers. Our value is reasonable because carbon electrode is a low efficient catalyst for oxygen reduction reaction, and oxygen reduction is only one of the possible parasitic reactions. Carbon oxidation in CDI is a complicated electrochemical process and the reaction kinetics is not well studied in literature. Despite the limited data available, our fitted parameters are comparable to those reported in porous carbon supercapacitor literature.[7]

Figure S-5a shows a comparison between experimental data and our leakage resistor element model. Here, the current is the parasitic current through each leakage resistor and voltage is the voltage across one electrode (from the leakage current experiments). Figure S-5b compares simulated total parasitic currents from LTspice model after implementing non-linear leakage resistor to experimental data. The simulation data agree well with experimental data, which validates the fitting procedures.

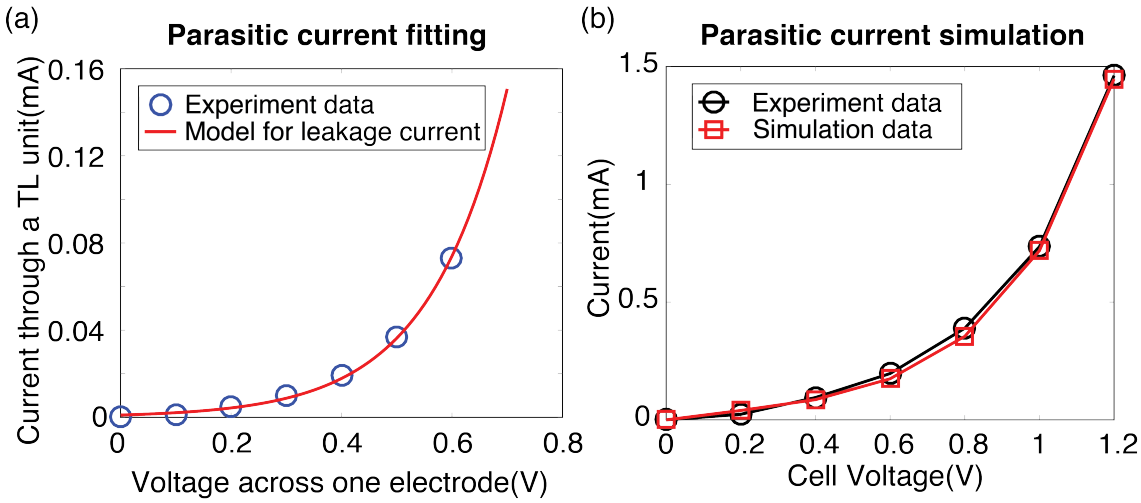

Figure S-5. a) Fitting experiment data with Bulter-Volmer equation to characterize parasitic current through each leakage resistor element. Blue circles are experimental data and the red line represents the model for leakage current. b) Parasitic currents of the whole CDI cell simulated by LTspice model after implementing non-linear leakage resistors. The simulation data agree well with experimental data.

S-6 Comparison of input charge from experiments and simulations

Figure S-6 shows the comparison of input charge from experimental data and simulation results. Simulations consistently predict higher input charges than experiments because the model does not capture the dynamic changes of ionic resistances during desalination (particularly important for constant voltage operation for short duration times). Note that CC simulations use input current from experiments and so charge transferred matches exactly with experiments.

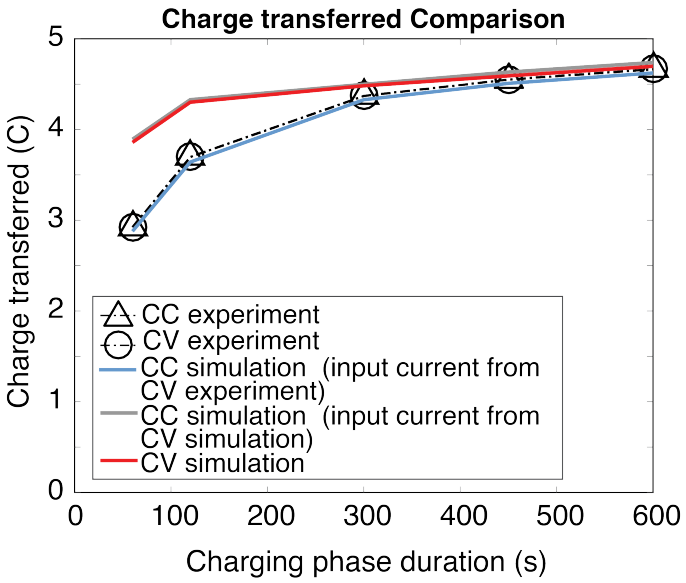

Figure S-6. Charge transfer comparison of experimental and simulation results of a ftCDI cell in CV or CC mode with charging times of 1, 2, 5, 7.5 and 10 min. CV and CC modes were operated under the conditions of the same input charges and identical charging phase timespans.

S-7 CDI cell electrode salt adsorption capacities

Figure S-7 shows the absolute salt adsorption capacities (in mg NaCl per g aerogel) of CV and CC modes with charging phase durations of 1, 2, 5, 7.5 and 10 min. The data presented here correspond to the data shown in Figure 4 in the main text. Within our ability to quantify this quantity, we observed no significance difference in salt absorption for the CC and CV modes.

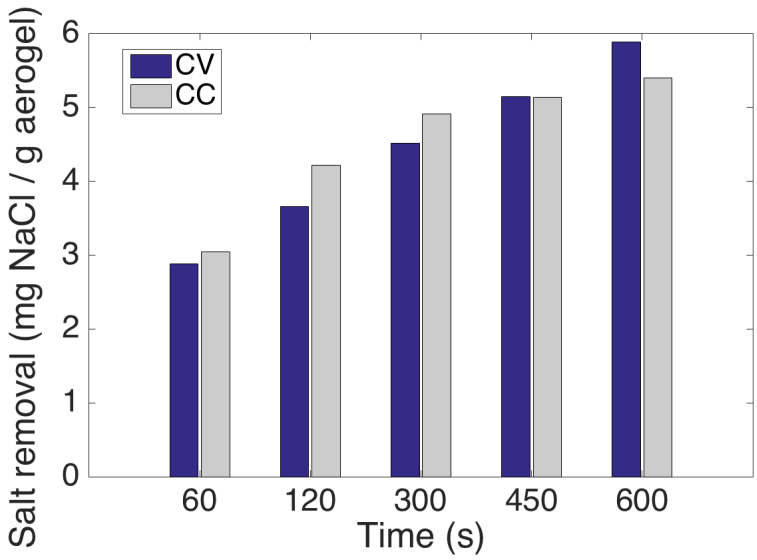

Figure S-7. Salt adsorption capacities of CV and CC modes (in mg NaCl per g aerogel) with charging phase durations of 1, 2, 5, 7.5 and 10 min.

REFERENCES

[1] M.D. Stoller, R.S. Ruoff, Best practice methods for determining an electrode material's performance for ultracapacitors, Energy & Environmental Science, 3 (2010) 1294.

[2] H. Wang, L. Pilon, Physical interpretation of cyclic voltammetry for measuring electric double layer capacitances, Electrochimica Acta, 64 (2012) 130-139.

[3] H. Wang, A. Thiele, L. Pilon, Simulations of Cyclic Voltammetry for Electric Double Layers in Asymmetric Electrolytes: A Generalized Modified Poisson–Nernst–Planck Model, The Journal of Physical Chemistry C, 117 (2013) 18286-18297.

[4] Y. Qu, T.F. Baumann, J.G. Santiago, M. Stadermann, Characterization of Resistances of a Capacitive Deionization System, Environ Sci Technol, 49 (2015) 9699-9706.

[5] M.E. Suss, T.F. Baumann, M.A. Worsley, K.A. Rose, T.F. Jaramillo, M. Stadermann, J.G. Santiago, Impedance-based study of capacitive porous carbon electrodes with hierarchical and bimodal porosity, Journal of Power Sources, 241 (2013) 266-273.

[6] Chaojie Song, J. Zhang, PEM Fuel Cell Electrocatalysts and Catalyst Layers: Fundamentals and Applications, in, Springer, 2008, pp. 89-134.

[7] T. Tevi, A. Takshi, Modeling and simulation study of the self-discharge in supercapacitors in presence of a blocking layer, Journal of Power Sources, 273 (2015) 857-862.